journal

J. Am. Ceram. Soc., **81** [10] 2661–69 (1998)

Elastic Anisotropy of β-Silicon Nitride Whiskers

Jack C. Hay,*,†,‡ Ellen Y. Sun,*,† George M. Pharr,*,§ Paul F. Becher,*,† and Kathleen B. Alexander*,†

Oak Ridge National Laboratory, Oak Ridge, Tennessee 37831

Department of Materials Science, Rice University, Houston, Texas 77005–1892

The elastic anisotropy of β-silicon nitride was examined using nanoindentation techniques. A coarse-grained polycrystalline sample composed of whiskers up to 15 μm in diameter and 100 μm in length allowed for the positioning of small indentations near the centers of grains, where neighboring grains minimally affect the property measurements. The crystallographic directions along which measurements were made were determined from the grain geometries in polished sections. The primary directions of interest were parallel to the *c*-axis (indenter penetration parallel to the whisker axis) and in the basal plane (indenter penetration perpendicular to the whisker axis), for which the indentation moduli were found to be 450 and 310 GPa, respectively. An indentation mechanics model used to estimate the single-crystal elastic constants from the nanoindentation results shows that Young's moduli for β-silicon nitride, which are similar to but not exactly the same as the moduli measured by nanoindentation techniques, vary from 540 GPa parallel to the *c*-axis to 280 GPa perpendicular to it. Hardness data, which also exhibit a strong anisotropy, are also presented.

I. Introduction

For many years silicon nitride has been the focus of ceramists in their search for a high-strength, high-toughness material for elevated-temperature applications such as gas turbines. Important developments in silicon nitride as a structural ceramic first occurred in the 1950s with the identification of the two polymorphs:[1,2] the alpha (α) and beta (β) phases. By nitriding silicon metal in a nitrogen or ammonia environment at 1350° to 1450°C, Ruddlesden and Popper[3] first produced α-silicon nitride, and others subsequently discovered[2,4–6] that heat treatment of α at temperatures in excess of 1500°C induces a phase transformation to β. Ruddlesden and Popper[3] and Hardie and Jack[7] obtained X-ray diffraction data characterizing the hexagonal crystal structures and lattice constants of both materials. Another important development was the discovery that the porosity occurring in both hot-pressed and reaction-bonded silicon nitride[8–12] can be significantly reduced by the addition of sintering aids which form intergranular phases, both glassy[13–20] and crystalline.[21–23] The second phase additions also promote the growth of long, whiskerlike grains of the β phase.

The fact that silicon nitride exists in at least two stable polymorphs has important consequences for its mechanical properties. Lange,[24,25] in a study of the relations between the relative amounts of the α and β phases and the strengths and fracture energies of polycrystalline silicon nitride, found that the long whiskerlike morphology of β grains leads to improved fracture toughness. These observations have now been linked to an *R*-curve behavior in the material,[25] and much of the current work in silicon nitride development focuses on increasing the size and volume fraction of the β whiskers to produce greater pullout loads and displacements.[22,26–29]

Central to a complete understanding of the mechanical behavior of silicon nitride ceramics is the elastic behavior. Young's moduli for polycrystalline silicon nitride have been evaluated by a variety of common techniques, including strain-gaged bend bars,[24,30] ultrasonic time of flight,[31] and resonance techniques.[20,32] Typical values reported in the literature are summarized in Table I. The polycrystalline Young's moduli typically fall in the range 300–330 GPa, with the exact value depending on porosity, intergranular phase content, texture, and the relative amounts of α and β.

While most measurements of the elastic properties of silicon nitride have been performed on polycrystalline specimens for which the behavior is usually assumed to be isotropic, the complex hexagonal crystal structures of silicon nitride suggest that in single-crystal form the materials may be elastically anisotropic, and a knowledge of this anisotropy is potentially important in many modeling situations. For example, Becher *et al.*,[35] in a recent study of crack propagation in an oxynitride glass reinforced with long whiskers of β-silicon nitride, found that the crack path depends on complex elastic interactions between the matrix and whiskers. Because anisotropic elastic constants were not available at the time of the study, polycrystalline average Young's moduli were used for the calculations, producing some uncertainty in the results. As another example, Zhou and Mitchell[36] and Reimanis *et al.*[37] recently examined dislocation activity and indentation fracture in large single crystals of α-silicon nitride grown by chemical vapor deposition. Since each of these phenomena is influenced by elastic anisotropy, use of a polycrystalline average Young's modulus to analyze and interpret the data may artificially enhance or mask important effects.

While it is possible to fabricate relatively large crystals of α, single crystals of β-silicon nitride large enough for complete elastic constant characterization by conventional methods have

Table I. Typical Young's Moduli for Polycrystalline Silicon Nitride

Ref.	*E*	Comments
24	307	
30	307	
31	315–332	Textured sample
20	192–320	Range of SiAlON compositions
32	303–317	Different volume fractions of β
33	310	Method not reported
34	380	Method not reported

J. E. Ritter, Jr.—contributing editor

Manuscript No. 190701. Received September 19, 1997; approved January 8, 1998.

*Member, American Ceramic Society.
†Oak Ridge National Laboratory.
‡Present address: IBM T. J. Watson Research Center, Yorktown Heights, New York 10598–0218.
§Rice University. Present address: Department of Materials Science and Engineering, University of Tennessee, Knoxville, Tennessee 37996–2200.

not yet been synthesized. Examination of elastic anisotropy in β-silicon nitride thus requires a specialized technique by which elastic properties can be probed in small, individual grains. Nanoindentation is one such technique. Developed largely over the past decade,[38] nanoindentation has been used to measure Young's modulus and the hardness of thin films, isolated phases, and individual grains as small as a few micrometers. With a good nanoindentation testing system, indentations can be positioned with a spatial resolution of approximately 1 μm, and it is possible to measure mechanical properties from indentations as shallow as 40 nm.

In the present study, nanoindentation techniques were used to estimate the single-crystal elastic constants of β-silicon nitride and characterize the anisotropy in its elastic behavior. The sample used for the study had long, whiskerlike grains approximately 15 μm in diameter and 100 μm in length. Nanoindentations were made in directions parallel to and perpendicular to the whisker axis, with the exact crystallographic orientation established by examination of the grain shape in the polished plane of the specimen. Results of the investigation show that there is a significant anisotropy in the Young's modulus as well as the hardness.

II. Experimental Procedure

(1) Materials

All measurements were performed on a coarse-grained, polycrystalline silicon nitride[¶] specimen with large β whiskers averaging 15 μm in diameter and 100 μm in length prepared by gas-pressure sintering. The starting powders for the specimen consisted of a high α-content Si_3N_4 with some β-Si_3N_4. To promote the transformation of α to β and to assist in the growth of long β whiskers, the silicon nitride was doped with approximately 2–3% alumina and 6–10% yttria. The powders were homogenized by attrition milling in 2-propanol for 4 h and isostatically pressed into green compacts at 630 MPa. The green compacts were gas-pressure sintered at a peak temperature of approximately 1900°C in nitrogen gas at 10 MPa for roughly 3 days. The exact temperature–pressure–time schedule for the sintering of the sample was not recorded as the furnace was allowed to cool at night while unattended.

Although the sintering additives aid in the growth of high aspect ratio β-whiskers,[39] the aluminum and oxygen ions they contain are also soluble in silicon nitride. To determine the extent to which the chemical composition of the material was altered from Si_3N_4, chemical characterization of several whiskers was performed in a scanning electron microscope (SEM) using energy dispersive X-ray spectroscopy. Since yttrium is not soluble in silicon nitride, and the oxygen and aluminum ions must be present in a manner which maintains electrical neutrality, only the aluminum ion concentration was explored. Denoting the aluminum ion concentration by z in the formula $Si_{6-z}Al_zO_zN_{8-z}$, the aluminum content in a few whiskers was found to be only as high as $z = 0.24$. This represents a substitution of approximately 4% aluminum ions for silicon ions. However, assuming the trends in elastic modulus for different SiAlON compounds observed by Tanaka *et al.*[20] apply to the whiskers tested here, the 4% aluminum ion concentration would be expected to reduce Young's modulus from that of pure Si_3N_4 by only 2.5%. A reduction in Young's modulus of this magnitude is within the range of experimental scatter.

To prepare the specimen for nanoindentation, standard metallographic techniques were employed to provide a flat, near-mirror polish with limited grain pullout. The sample was rough ground using 125 and 40 μm Struers diamond pads, and fine ground using a 6 μm Struers Petrodisc-M and a 6 μm Petrodisc. Final polishing was accomplished using progressively finer diamond pastes, from 3 to 0.5 μm, and a glycol-based lubricant. Optical microscopy revealed a very flat surface with a few regions where grains, or groups of grains, had been pulled out.

(2) Methods

All indentation experiments were conducted using a Nanoindenter II (Nano Instruments, Inc., Oak Ridge, TN) capable of measuring both the applied indentation loads and the total penetration depths during an indentation experiment. In this instrument, a three-plate capacitive displacement gage measures the penetration depth with a resolution of 0.04 nm, and the loading mechanism, which consists of a large permanent magnet and a small coil, has a resolution of 75 nN. However, the accuracy of the measured properties is limited by other factors such as surface preparation and electronic noise. Although the instrument is theoretically capable of a spatial positioning resolution of 0.4 μm, the optical microscope used for locating indentation sites limits the practical positioning resolution to about 1 μm. The benefit of simultaneously measuring the loads and displacements during indentation is that the elastic modulus and hardness, as determined by the Oliver–Pharr method,[38] can be measured without direct imaging of the indentations.

All indentation experiments were performed using the three-sided Berkovich diamond tip. By positioning the indentations in the centers of large grains, properties were measured in a manner which was minimally affected by the neighboring grains and glassy phases.

The data obtained in the nanoindentation experiments were analyzed to determine the indentation modulus and hardness using the Oliver–Pharr method.[38] The quantities of interest, which were obtained directly from the raw data or derived from it, include the peak load, P_{max}, the peak displacement, h_{max}, the contact depth, h_c, the contact area, A_c, and the contact stiffness, S. For the indentation data studied in this paper, 50% of the unloading curve was fitted to the power law relation described by Oliver and Pharr to determine the contact stiffness. The relations used to compute the hardness, H, and the effective indentation modulus, E_{eff}, from the measured quantities are

$$H = \frac{P_{max}}{A_c} \tag{1}$$

$$E_{eff} = \frac{\sqrt{\pi}}{2} S \frac{1}{\beta} \frac{1}{\sqrt{A_c}} \tag{2}$$

Equation (2), which follows from an analytical solution derived by Sneddon for the penetration of an elastic half space by an axisymmetric indenter of arbitrary smooth profile,[40,41] relates the experimental stiffness and the contact area to the effective elastic modulus. The constant, β, a correction factor approximately equal to 1.034 for the Berkovich indenter,[42] accounts for the geometrical difference between the triangular cross section of the Berkovich indenter and the circular cross section of axisymmetric indenter treated by Sneddon. The indentation modulus, E, is obtained from the effective modulus using

$$E = \frac{1 - \nu^2}{\dfrac{1}{E_{eff}} - \dfrac{1 - \nu_i^2}{E_i}} \tag{3}$$

where ν_i and E_i are the elastic properties of the diamond indenter. The indenter properties used for all calculations were $\nu_i = 0.07$ and $E_i = 1140$ GPa. It is important to note that if the material is elastically isotropic, the indentation modulus derived using this methodology is the same as Young's modulus. However, as will be discussed in greater detail in the Discussion section, this is not necessarily the case for an anisotropic material.

Two sets of indentation experiments were conducted: one for

¶Provided by Michael J. Hoffmann, University of Karlsruhe, Germany.

the calibration of the indenter shape function, which relates the cross-sectional area of the indenter to the distance from the diamond apex (also called the indenter area function), and a second set to measure the indentation modulus and hardness of β-silicon nitride. Fused quartz, an elastically isotropic material with a relatively low Young's modulus and a moderate hardness, was used for calibrating the shape function. As shown in Fig. 1, the shape function was chosen so that Young's moduli for fused quartz derived from the indentation load–displacement data were 72 GPa[43] at all indentation depths. To validate the shape function, a similar set of experiments was performed on a polycrystalline tungsten sample, which has a modulus similar to that of silicon nitride but is elastically isotropic. The tungsten data, which are also plotted in Fig. 1, confirm the validity of the shape function by virtue of the agreement between the data and the dashed line representing the known Young's modulus of tungsten, 411 GPa.[44] The deviations in the tungsten modulus at small contact depths result from relief texture on the specimen surface produced during mechanical polishing, an artifact absent in the near-mirror polish on the silicon nitride.

The properties of the silicon nitride whiskers were measured using a two-part experimental indentation procedure which provided elastic modulus and hardness information at two different indentation depths at the same location on the specimen. In the first experiment, the indenter approached the surface at 10 nm/s and penetrated the specimen at a constant loading rate of 0.2 mN/s to a maximum load of 4 mN. The load was then held constant at maximum load for 10 s, followed by a 90% load reduction at a rate of 0.2 mN/s. After the load was held constant for 100 s, the second experiment was performed by loading the indenter to the larger peak load of 120 mN at the same specimen location and then completely unloading. The primary function of the larger, higher load indentation (120 mN) was to produce a large hardness impression from which the location of the indentation within the grain could be verified by SEM observation. Data obtained from the smaller 4 mN indentations, which penetrated the silicon nitride surface to only about 10–70 nm, will be used for most analyses since they are less influenced by neighboring grains and intergranular phases.

Approximately 200 indentations were produced using the two-step procedure. Whiskers were chosen for measurement based on their orientation, which was deduced from the grain geometry in the plane of polish. The hexagonal crystal symmetry produces nearly perfect hexagonal grain shapes for whiskers aligned with the *c*-axis perpendicular to the specimen surface, whereas whiskers aligned with the *c*-axis parallel to the surface appear as long thin rectangles. Numerous whiskers in each of the orientations were tested. Figure 2 is an SEM micrograph depicting several indentations in a single whisker with its *c*-axis parallel to the plane of polish. Close inspection of the micrograph shows that one indentation produced cracking near a grain-boundary pore. Approximately 75% of the indentations produced cracks or resided on or near a grain boundary and were removed from the data set presented in the Results.

III. Results

The indentation moduli evaluated by nanoindentation techniques for directions parallel and perpendicular to the *c*-axis are shown in Fig. 3. The figure includes data obtained at both peak loads used in the two-part indentation procedure, 4 and 120 mN. Note that the contact depths for the lower load indentations, which are roughly 60 to 70 nm deep, exhibit a relatively small variation, whereas for the higher load indentations, the contact depths are scattered over a much larger range, 400–550 nm. Because of the larger variations in contact depth and a greater propensity for indentation cracking at the larger loads, more confidence is placed in the lower load data, and all further analyses and discussions are limited to the low load measurements.

Inspection of Fig. 3 shows that the indentation moduli measured at low loads are separated into two distinct groups based on crystallographic direction, consistent with the notion that the material is elastically anisotropic. The indentation moduli are lower for the indentations made perpendicular to the *c*-axis (parallel to the basal plane), with values clustering in the range 310–340 GPa range. Since the specific testing directions within the basal plane were essentially random, this relatively narrow range of moduli suggests that β-silicon nitride is nearly isotropic in the basal plane, as would be expected for a material with hexagonal symmetry.[45] For indentations made parallel to the *c*-axis, higher moduli were observed, with values ranging from 312 to 450 GPa. As will be discussed shortly, the much greater variability in these data is not due to instrumental scatter, which can account for only about a 2% variation for indentations made in this load and size range, but is a real material effect resulting from a sensitivity of the indentation modulus to

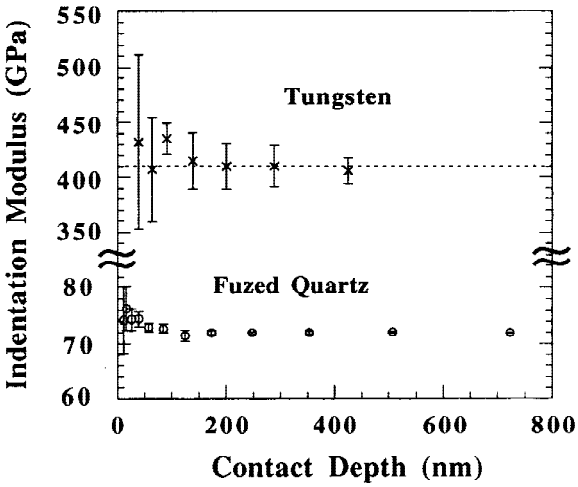

Fig. 1. Indentation modulus of fused quartz and tungsten versus contact depth. The fused quartz data were used to calibrate the shape function of the diamond indenter. Note the broken vertical scale.

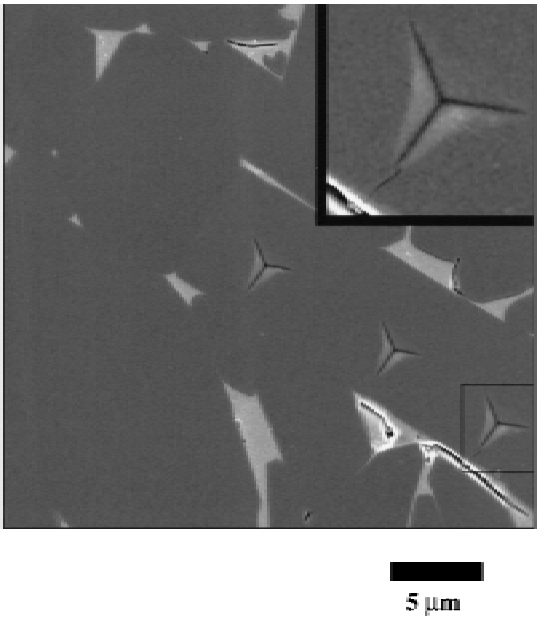

Fig. 2. Scanning electron micrograph of indentations made perpendicular to the whisker axis. The close-up depicts the cracking which occurred at some indentations.

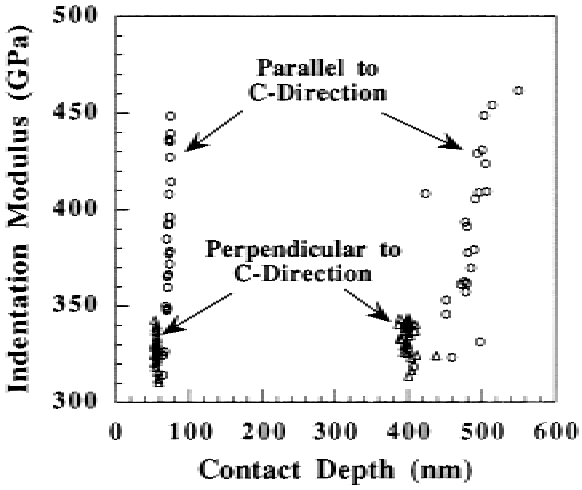

Fig. 3. Indentation modulus results for β-silicon nitride indicating the substantial anisotropy in the two primary crystallographic directions. The two-step loading procedure yielded measurements at two contact depths (60 and 450 nm).

the precise crystallographic orientation along which the indentation was made.

The difference between the indentation moduli in the two crystallographic directions suggests that there may indeed be a measurable elastic anisotropy in the material. However, it is also possible that the separation of the data into two groups is caused by an influence of the glassy intergranular phase. As depicted in Fig. 4, the modulus of a two-phase material measured in an indentation experiment is strongly influenced by the material directly beneath the indenter. Since the whiskers were tens to hundreds of micrometers in length, the glassy phase would only weakly affect measurements parallel to the *c*-direction (left side of Fig. 4). On the other hand, measurements performed perpendicular to the whisker axis would be expected to be more sensitive to second-phase influences, since in this orientation the glassy phase lies at a distance of only a fraction of a whisker diameter directly beneath the indenter (right side of Fig. 4). If the elastic modulus of the glassy phase is relatively low, a reduction in indentation modulus more pronounced in directions perpendicular to the whisker axis than parallel to it would result, consistent with the data in Fig. 3.

An elastic analysis of indentation in films on substrates by Gao *et al.*[46] can be used to estimate the limiting influences of the glassy phase under these circumstances. In Gao's model, the indentation modulus is determined as a function of a/t where a is the radius of the flat-ended punch pressing against a film of thickness, t. In order that the modeled behavior can be compared directly with the experimental data, an assumption of a perfect conical tip allows one to model the indentation modulus as a function of h_c/t, where h_c is the contact depth. Therefore, the film properties dominate the measured modulus at very shallow indentation depths, but both the film and the substrate properties influence the modulus measurement when the contact depth approaches the film thickness.

In Fig. 5, the composite indentation modulus of a silicon nitride film with an assumed modulus of 450 GPa on an infinite glass substrate with an assumed modulus of 140 GPa has been computed using Gao's analysis and is plotted for three different film thicknesses. The film thickness of 7000 nm corresponds to about half of a whisker diameter, an estimate of the film thickness for a whisker lying parallel to the surface. The other two film thicknesses, 4000 and 2000 nm, represent cases where the plane of polish is not through the center of the whisker and the effective film thickness is smaller. The 140 GPa Young's modulus assumed for the glassy phase is representative of a typical Si–Al–Y oxynitride glass[47] which may be observed in silicon nitride ceramics doped with yttria and alumina.

The results in Fig. 5 demonstrate that a large amount of a low modulus glass directly beneath the whisker could indeed reduce the indentation modulus by a significant and measurable amount, but only for contact depths greater than about 100 nm. At the 60–70 nm depths at which the experimental data were obtained, the reduction in modulus is at most 4%, even when the silicon nitride film is only 2000 nm thick. Since the sample does not contain large quantities of glass, this is a very conservative estimate of the modulus reduction. In fact, inspection of Fig. 3 suggests that the glassy phase does not influence the indentation modulus even at the larger contact depths of 400–500 nm since the indentation modulus does not differ significantly from that at 60–70 nm. It is therefore concluded that the separation of the indentation modulus data in Fig. 3 is due to elastic anisotropy in the material.

As mentioned previously, the wide variation in indentation modulus for measurements made parallel to the *c*-direction of the crystal is due to a sensitivity of the indentation modulus to the precise orientation of the whisker's *c*-axis relative to the normal for the polished surface. An attempt was made to identify the exact crystallographic orientation of the silicon nitride whiskers with respect to the polished surface by electron backscattering patterns (EBSP). However, difficulties were encountered in sputtering a conductive coating on the sample which

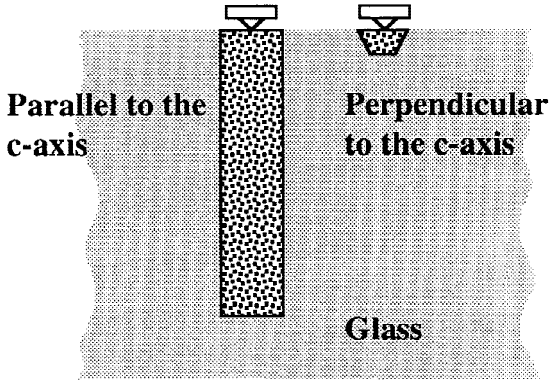

Fig. 4. Schematic representation of the two whisker orientations used for indentation experiments. Parallel to the *c*-axis, the indentation measurement is not strongly affected by the presence of glass. Perpendicular to the *c*-axis, large indentations may be affected by the glassy phase.

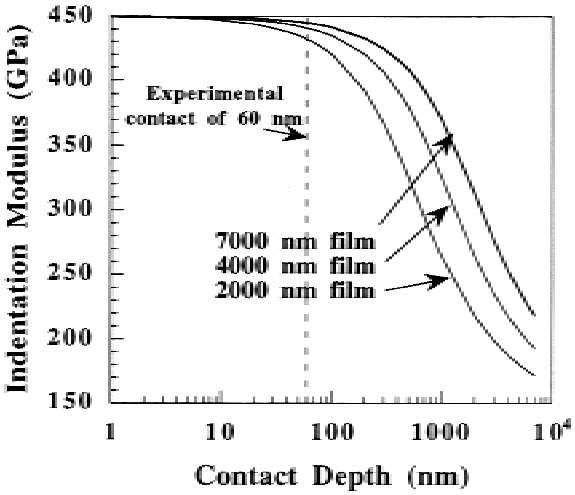

Fig. 5. Indentation modulus predicted from Gao's elastic analysis assuming a thin film of silicon nitride ($E = 450$ GPa, $\nu = 0.24$) on an infinite half-space of glass ($E = 140$ GPa, $\nu = 0.22$).

was thick enough to prevent charging, yet thin enough to obtain identifiable diffraction patterns.

As an alternative means for estimating the whisker orientation, images of the whisker cross sections provided the desired information. As shown in Fig. 6, the whiskers selected for *c*-axis measurement were identified by the characteristic hexagonal cross section produced by the crystal symmetry. Whereas the whisker in Fig. 6 is nearly a perfect hexagon, most whiskers were tilted slightly off-axis producing an elongation and distortion of the hexagonal geometry, an example of which is shown in Fig. 7. From measurements of micrographs like that in Fig. 7, the distortion of the hexagon can be used to determine the off-axis tilt angle, α, defined by the geometry shown in Fig. 8. The specific procedure developed for this study is based on the triangles formed by the tangents to the sides of the whisker. Referring to Fig. 6, the tangents to the hexagonal sides of a whisker oriented nearly perpendicular to the polished surface form equilateral triangles with angles of 60° and sides of equal length. On the other hand, for whiskers intersecting the surface through a small rotation and tilt, the triangles are not equilateral. It follows from three-dimensional geometry that measurements of the angles and lengths of sides of the triangles, such as those shown in Fig. 7, can be used to deduce the off-axis tilt angle, α. Details of the geometry and procedure used for this calculation are given in the Appendix. By examining SEM micrographs like those in Figs. 6 and 7 in which tangents could clearly be drawn on the whisker boundaries, the tilt angles of the whisker axes were determined.

The dependence of the indentation modulus on the tilt angle is plotted in Fig. 9, showing that the indentation modulus decreases from 450 GPa in the *c*-direction to roughly 310 GPa in directions perpendicular to it. The well-behaved trend in the data when plotted this way suggests that the large indentation modulus variation in Fig. 3 is not scatter, but rather results from strong crystal anisotropy and a resulting sensitivity of the indentation modulus to off-axis tilt.

Finally, the hardnesses measured at the lower indentation load and depth (~60 nm) are shown in Fig. 10. Like the modulus, the hardness is also anisotropic, varying from a minimum of about 19 GPa for indentations made parallel to the *c*-axis to a maximum of 35 GPa perpendicular to the *c*-axis. It is interesting to note that the trend in hardness anisotropy runs exactly

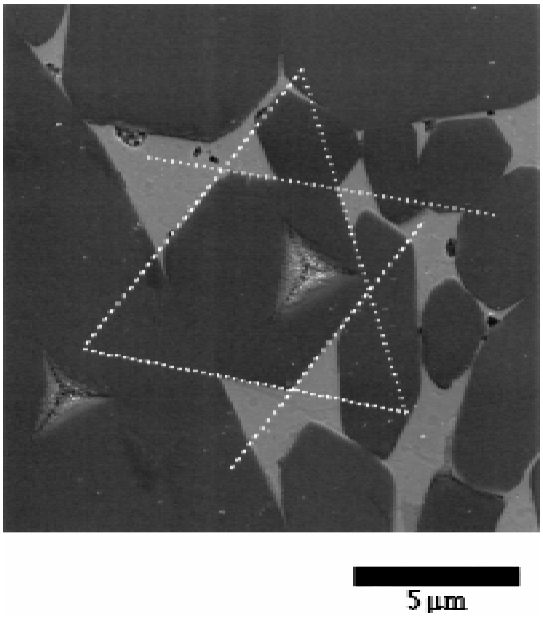

Fig. 6. Scanning electron micrograph of a whisker oriented nearly perpendicular to the polished surface. The tangents to the grain boundaries, shown as dashed lines, form equilateral triangles characteristic of a regular hexagon.

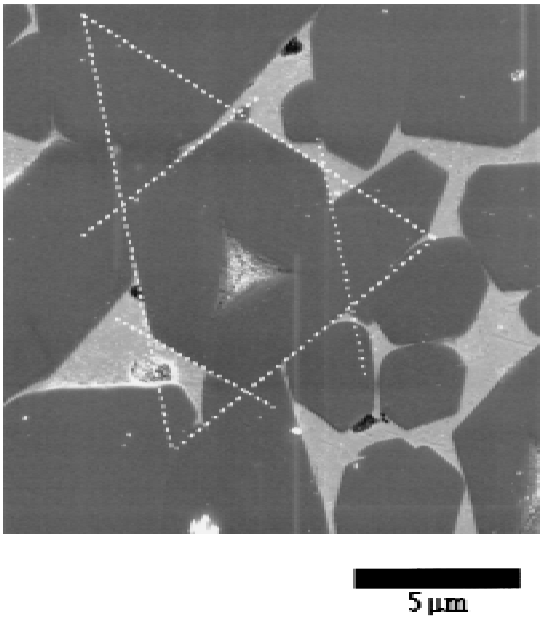

Fig. 7. Scanning electron micrograph of a whisker which is not oriented perpendicular to the polished surface. The tangents to the boundaries, shown as dashed lines, do not form the equilateral triangles characteristic of a regular hexagon.

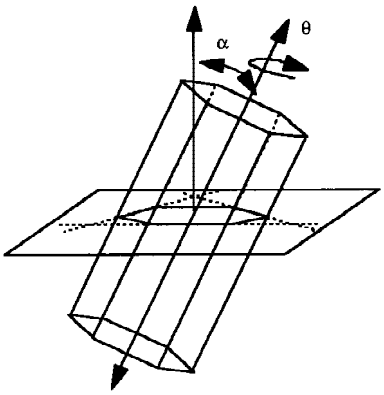

Fig. 8. Geometry used to determine the tilt angle, α, from grain boundary tangents, such as those drawn on Figs. 6 and 7.

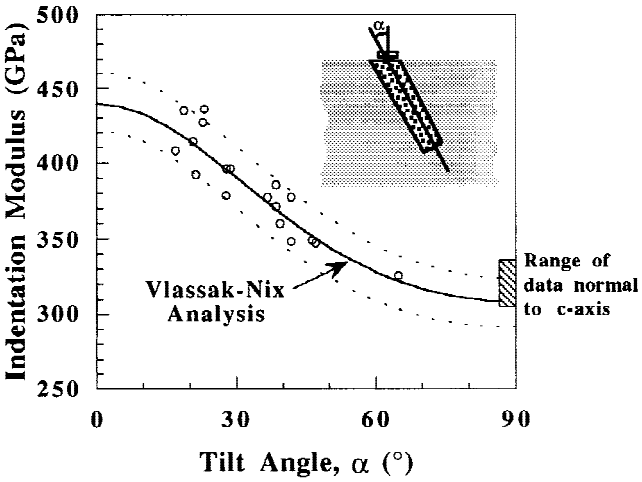

Fig. 9. Indentation modulus plotted as a function of tilt angle. The solid line represents the indentation modulus calculated using the Vlassak–Nix analysis and the single-crystal elastic constants. The dashed lines represent possible deviations due to uncertainties in the Poisson ratios.

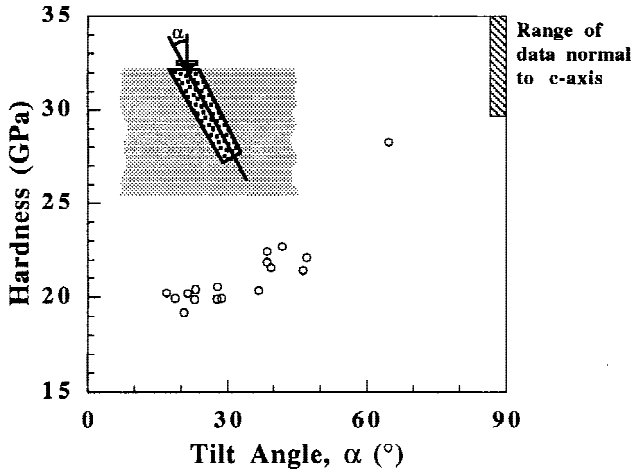

Fig. 10. Hardness plotted as a function of tilt angle. The hardness appears to vary from 19 GPa in indentation direction parallel to the *c*-direction to 30–35 GPa normal to the *c*-direction.

opposite to that of the modulus; that is, the direction of highest modulus corresponds to lowest hardness and vice versa.

IV. Discussion

To this point, the elastic moduli reported in this work have been deliberately referred to as ''indentation moduli'' rather than ''Young's moduli.'' The reason for this distinction, as alluded to previously, is that the data analysis procedures used to obtain indentation moduli from the nanoindentation load–displacement data are based on contact mechanics solutions for elastically isotropic media and therefore formally apply only to isotropic materials.[38] An important consequence is that the indentation modulus measured in a specific crystallographic direction in a nanoindentation experiment will be the same as Young' modulus in that direction only if the material is elastically isotropic. For anisotropic materials, the indentation modulus is, in general, different from Young's modulus, with its value depending on all of the elastic constants of the material in a complex way. Fortunately, for relatively blunt indenters like the Berkovich pyramid used in a great deal of nanoindentation work, the indentation modulus is usually strongly biased toward Young's modulus and provides a useful first-order approximation of it. However, when greater measurement accuracy is required, other analytical procedures must be employed.

Vlassak and Nix[48,49] have recently developed a method for determining the indentation modulus of a general anisotropic solid in any crystallographic direction from its single-crystal elastic constants. In this method, the indentation contact is modeled by a rigid, flat-ended punch pressed against an infinite anisotropic medium, and the indentation modulus, as defined by Eqs. (2) and (3), is related to the single-crystal elastic constants through integral expressions that can be numerically evaluated. Experiments performed by Vlassak and Nix demonstrated that their method accurately models the indentation moduli of many cubic and hexagonal single crystals.

By making several simplifying assumptions, the Vlassak–Nix method can be used in reverse to estimate the anisotropic elastic constants of β-silicon nitride from the indentation modulus data in Fig. 9. Elasticity in a hexagonal material is described by five independent elastic constants, which can be taken as either the single-crystal stiffness coefficients c_{11}, c_{12}, c_{13}, c_{33}, and c_{44}, or the engineering coefficients, E_x, E_z, ν_{xy}, ν_{zx}, and G_{xz}.[50] For this development, the engineering constants will be used, with the stiffnesses presented later. The symbols E, ν, and G represent Young's moduli, Poisson ratios, and shear moduli, respectively, with the subscripts x, y, and z denoting the direction or plane in which the quantities are defined. The x–y plane corresponds to the basal plane of the hexagonal crystal, and the c-axis of the crystal coincides with z.

In the interest of reducing the number of unknown parameters, one can ascribe physical significance and limits to some of the unknown quantities. Table II presents some data from Simmons and Wang[51] for several hexagonal materials: cobalt, erbium, hafnium, magnesium, titanium, yttrium, and zirconium. Like silicon nitride, all have hexagonal crystal structures and all have a higher stiffness in the c-direction than in the basal plane. Inspection of the data in the table shows that the Poisson ratios for these materials do not vary widely, but rather lie in the fairly narrow ranges $0.30 \leq \nu_{xy} \leq 0.47$ and $0.19 \leq \nu_{zx} \leq 0.32$. Thus, as a first approximation, it will be assumed that $\nu_{xy} = 0.35$ and $\nu_{zx} = 0.25$, but it will later be shown that the computed indentation moduli do not depend strongly on the exact values chosen for the Poisson ratios as long as they are within these ranges. This assumption, which reduces the number of unknowns from five to three, is similar to what is usually done in the analysis of nanoindentation data for an isotropic material. That is, to derive Young's modulus, a value for Poisson's ratio must be assumed (see Eqs. (2) and (3)).

The number of unknown quantities can be reduced further by assuming a simple relation between the shear modulus, G_{xz}, and the other elastic constants. Although strictly speaking G_{xz} is independent of the other constants, examination of the single-crystal constants in Table II shows that

$$0.80 < G_{xz}\frac{2(1+\nu_{xz})}{E_x} < 1.06 \tag{4}$$

The above parameter is chosen because its counterpart for an isotropic material is exactly 1. According to Table II, the parameter is also close to unity for many hexagonal materials. Thus, by assuming that

$$G_{xz} = \frac{E_x}{2(1+\nu_{xz})} \tag{5}$$

the number of unknown parameters is reduced to two.

The two remaining constants, E_x and E_z, were treated as fitting parameters and systematically varied to obtain the best correlation between the predictions of the Vlassak–Nix model and the experimental indentation modulus data in Fig. 9. The best fit was achieved using the elastic constants summarized in Table III, which includes both the engineering coefficients and

Table II. Elastic Properties of Several Materials Possessing the Hexagonal Crystal Structure[52]

Material	E_x	E_z	ν_{xy}	ν_{zx}	G_{xz}	$G_{xz}[2(1+\nu_{xz})/E_x]$
Cobalt	160.54	197.75	0.45	0.32	52.00	0.82
Erbium	72.85	76.72	0.30	0.19	28.09	0.91
Hafnium	139.86	163.08	0.35	0.26	55.70	0.97
Magnesium	44.84	50.51	0.35	0.23	16.81	0.90
Titanium	106.94	144.40	0.47	0.27	47.20	1.06
Yttrium	65.73	69.82	0.32	0.19	24.56	0.88
Zirconium	100.87	126.33	0.39	0.30	32.40	0.80

Table III. Estimated Single-Crystal Elastic Constants for β-Silicon Nitride

Engineering coefficients	Stiffness coefficients
E_x = 280 GPa	c_{11} = 343 GPa
E_z = 540 GPa	c_{12} = 136 GPa
ν_{xy} = 0.35	c_{13} = 120 GPa
ν_{zx} = 0.25	c_{33} = 600 GPa
G_{xz} = 124 GPa	c_{44} = 124 GPa

the stiffness coefficients derived from them. The fit, which is shown as the solid curve through the data points in Fig. 9, provides a good description of the trends in the experimental data. Note that although the indentation moduli calculated at $\alpha = 0°$ and 90° depend on both E_x and E_z, the indentation modulus at 90° is dominantly controlled by $E_x = 280$ GPa and the modulus at 0° by $E_z = 540$ GPa.

To systematically examine the sensitivity of the calculations to the assumed Poisson ratios, the indentation moduli were recomputed allowing ν_{xy} and ν_{zx} to take on all possible combinations of 0.1, 0.2, 0.3, 0.4 while maintaining E_x and E_z constant. The lower dashed curve in Fig. 9 represents the indentation modulus derived assuming both Poisson ratios to be 0.1, and the upper curve was calculated assuming both equal to 0.4. Other combinations affected the shape of the curve, but the dashed lines were found to represent the absolute upper and lower limits, approximately ±5%. The indentation moduli are thus not especially sensitive to the choice of the Poisson ratios in the range 0.1 to 0.4.

To emphasize the difference between the indentation moduli and Young's moduli, values computed from the elastic constants in Table III are compared in Fig. 11. The indentation moduli were determined by the Vlassak–Nix method[48,49] and Young's moduli using standard methods found in elasticity texts (e.g., Ref. 45). The indentation modulus in the stiffest direction ($\alpha = 0°$, i.e., the *c*-axis of the crystal) underestimates the single-crystal Young's modulus by about 20%, and in the most compliant direction, overestimates Young's modulus by about 10%. Thus, as noted earlier, Young's modulus in the direction of indentation dominates the indentation modulus, but the indentation modulus still depends to some extent on the other elastic constants.

The data in Fig. 11 also provide a measure of the magnitude of the elastic anisotropy in β-silicon nitride. Young's moduli vary from 540 GPa parallel to the *c*-axis to 280 GPa perpendicular to it (i.e., in the basal plane), and thus by almost a factor of 2 in the two orthogonal crystallographic directions of primary interest in this study. This anisotropy is much greater than that reported recently by Lee and Bowman[31] for a textured β-silicon nitride polycrystal examined by more conventional methods. In that study, a polycrystalline sample was produced by hot-pressing silicon nitride with 10% MgO, which allowed for the transformation and rapid growth of the β-phase. Conventional ultrasonic techniques were implemented to measure Young's moduli in the directions parallel to the pressing direction (perpendicular to the *c*-axis) and in the hot-pressing plane. Young's moduli were reported as 332 and 315 GPa parallel and perpendicular to the pressing direction, respectively. The authors suggested that the small difference in Young's moduli could be due to low anisotropies in the single-crystal elastic constants, which appears to be inconsistent with the nanoindentation results. However, the pole figure presented by Lee and Bowman indicates that while the *c*-axes lie in the hot-pressing plane there is a random orientation of the whiskers in the plane. Therefore, Young's modulus for the hot-pressing plane can be related to the single-crystal elastic constants by averaging over all orientations in the plane. This polycrystalline, two-dimensional average is an average Young's modulus which can be evaluated from Fig. 11. In materials with the hexagonal symmetry this two-dimensional analysis yields 310 GPa, which is the same as the more conventional three-dimensional Reuss[52] procedure. Although silicon nitride exhibits a large elastic anisotropy, the polycrystalline average is low because of the rate at which Young's modulus decays between the *c*-axis and the directions perpendicular to the *c*-axis, as demonstrated in Fig. 11. The single-crystal constants presented in Table III are, therefore, consistent with the polycrystalline average presented by Lee and Bowman.

This analysis can be taken one step further by using the single-crystal elastic constants to estimate Young's modulus of a β-silicon nitride polycrystal having random orientation in all directions using the Voigt[53] and Reuss[52] averaging procedures. Using the constants in Table III, the upper and lower bounds of the polycrystalline Young's modulus are 329 GPa (Voigt) and 310 GPa (Reuss). This range is very consistent with the polycrystalline data in Table I, thus providing another independent check on the consistency of the estimated elastic constants.

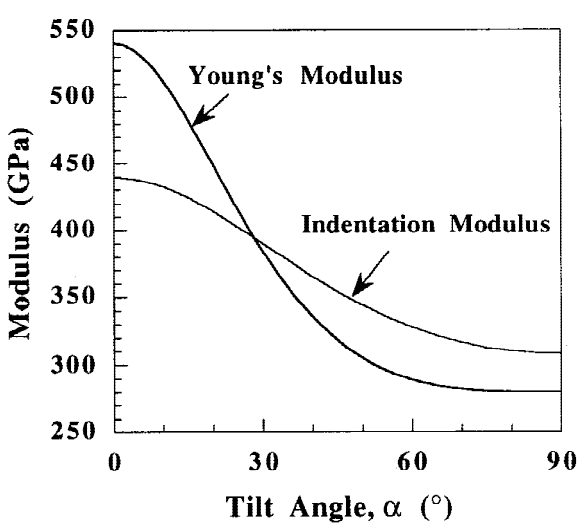

Fig. 11. Young's modulus calculated from the single-crystal elastic constants compared with the indentation modulus for the range of crystallographic directions.

V. Conclusions

Nanoindentation has been shown to be a useful tool for probing elastic anisotropy in materials which cannot be produced as single crystals large enough to be characterized by conventional measurement techniques. For anisotropic solids, the indentation modulus measured by nanoindentation techniques is different from Young's modulus, but by making simple assumptions about some of the elastic constants, an analysis developed by Vlassak and Nix analysis can be used to estimate the single-crystal elastic constants and Young's moduli from nanoindentation measurements.

Measurements performed on large whiskerlike grains of β-silicon nitride show this hexagonal material to be highly elastically anisotropic, with Young's modulus of approximately 280 GPa perpendicular to the *c*-axis (in the basal plane) and 540 GPa parallel to it. The strong elastic anisotropy has important implications for modeling mechanical phenomena in materials containing β-silicon nitride whiskers, and for the use of silicon nitride in engineering applications such as thin protective coatings grown as highly textured films.

APPENDIX

This Appendix provides details of the three-dimensional geometry which is used to determine the rotation angle and tilt angle of a hexagonal prism from an arbitrary intersecting plane. Referring to the schematic in Fig. A1, the lengths of the base, b_1, and the altitude, h_1, transform to

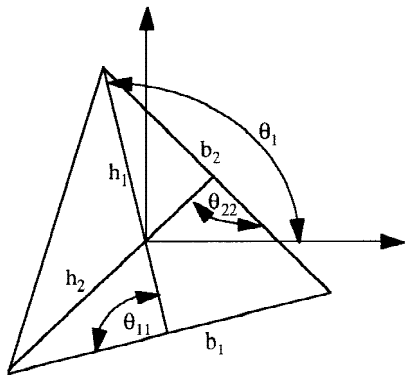

Fig. A1. Schematic of the altitudes, *h*, bases, *b*, and the characteristic angles measured from Figs. 6 and 7 used to evaluate the off-axis tilt angle, α.

$$\vec{h}_1 = \frac{\sqrt{3}}{2} L \cos\theta_1\, i + \frac{\sqrt{3}}{2} L \sin\theta_1 \cos\alpha j$$
$$\vec{b}_1 = -L \sin\theta_1\, i + L \cos\theta_1 \cos\alpha j \qquad \text{(A-1)}$$

where L is the length of the untransformed triangle side, θ_1 is the angle between the x-axis and the altitude, h_1, and i and j are unit vectors in the x and y directions. The scalar product of h_1 and b_1 is given by

$$\vec{h}_1 \cdot \vec{b}_1 = |h_1||b_1| \cos\theta_{11} = -\frac{\sqrt{3}}{2} L \sin\theta_1 \cos\theta_1 \sin^2\alpha \qquad \text{(A-2)}$$

where θ_{11} has been defined in Fig. A1. Similar expressions can be derived for a second side and altitude, b_2 and h_2, given by

$$\vec{h}_2 = \frac{\sqrt{3}}{2} L \cos\theta_2\, i + \frac{\sqrt{3}}{2} L \sin\theta_2 \cos\alpha j$$
$$\vec{b}_2 = -L \sin\theta_2\, i + L \cos\theta_2 \cos\alpha j \qquad \text{(A-3)}$$

for which the dot product gives

$$\vec{h}_2 \cdot \vec{b}_2\, |h_2||b_2| \cos\theta_{22} = -\frac{\sqrt{3}}{2} L \sin\theta_2 \cos\theta_2 \sin^2\alpha \qquad \text{(A-4)}$$

where the angle θ_2 is given by

$$\theta_2 = \theta_1 + 120° \qquad \text{(A-5)}$$

and θ_{22} has been defined in Fig. A1. From Eqs. (A-2), (A-4), and (A-5) the rotation angle is

$$\theta_1 = \frac{1}{2} \tan^{-1} \left[\frac{\sin(240°)}{\dfrac{|h_2||b_2| \cos\theta_{22}}{|h_1||b_1| \cos\theta_{11}} - \cos(240°)} \right] \qquad \text{(A-6)}$$

Finally, to evaluate the tilt angle, α, the scalar products for b_1 and b_2 give

$$\vec{b}_1 \cdot \vec{b}_1 = |b_1^2| = L^2 \sin^2\theta_1 + L^2 \cos^2\theta_1 \cos^2\alpha$$
$$\vec{b}_2 \cdot \vec{b}_2 = |b_2^2| = L^2 \sin^2\theta_2 + L^2 \cos^2\theta_2 \cos^2\alpha \qquad \text{(A-7)}$$

Eliminating the side length, L, from both equations results in a final expression for the tilt angle

$$\cos^2\alpha = \frac{|b_1^2| \sin^2\theta_2 - |b_2^2| \sin^2\theta_1}{|b_2^2| \cos^2\theta_1 - |b_1^2| \cos^2\theta_2} \qquad \text{(A-8)}$$

Substitution for the angle, θ_2, from Eq. (A-5) results in the final expression

$$\alpha = \cos^{-1} \{[|b_1^2|(\sin\theta_1 \cos(120°) + \sin(120°) \cos\theta_1)^2 - |b_2^2| \sin^2\theta_1]/[|b_2^2| \cos^2\theta_1 - |b_1^2|(\cos\theta_1 \cos(120°) - \sin\theta_1 \sin(120°))^2]\}^{1/2} \qquad \text{(A-9)}$$

from which the tilt angle can be determined from measurements of the rotation angle, θ_1, and the two base lengths, b_1 and b_2.

Acknowledgments: This research was sponsored in part by the Division of Materials Sciences, U.S. Department of Energy, under Contract No. DE-AC05-96OR22464 with Lockheed Martin Energy Research Corp., through the SHaRE Program under Contract No. DE-AC05-76OR00033 with Oak Ridge Associated Universities, and by an appointment (J.C.H.) to the ORNL Postdoctoral Research Associates Program administered jointly by the Oak Ridge Institute for Science and Education and Oak Ridge National Laboratory.

References

[1]E. T. Turkdogan and S. Ignatowicz, ''The Solubility of Nitrogen and Formation of Silicon Nitride in Iron–Silicon Alloys,'' *J. Iron Steel Inst.*, **185**, 200–206 (1957).

[2]E. T. Turkdogan, P. M. Bills, and V. A. Tippett, ''Silicon Nitrides: Some Physico-Chemical Properties,'' *J. Appl. Chem.*, **8**, 296–302 (1958).

[3]S. N. Ruddlesden and P. Popper, ''On the Crystal Structures of the Nitrides of Silicon and Germanium,'' *Acta Crystallogr.*, **11**, 465–68 (1958).

[4]R. Messier, L. Riley, and R. J. Brook, ''The α/β Silicon Nitride Phase Transformation,'' *J. Mater. Sci.*, **13**, 1199–205 (1978).

[5]W. D. Forgeng and B. F. Decker, ''Nitrides of Silicon,'' *Trans. AIME*, **212**, 343–48 (1958).

[6]D. S. Thompson and P. L. Pratt, *Science of Ceramics*, Vol. 3; p. 33. Edited by G. H. Stewart. Academic Press, New York, 1967.

[7]D. Hardie and K. H. Jack, ''Crystal Structures of Silicon Nitride,'' *Nature* (*London*), **180**, 332–33 (1957).

[8]G. R. Tewilliger and F. F. Lange, ''Pressureless Sintering of Si_3N_4,'' *J. Mater. Sci.*, **10**, 1169–74 (1975).

[9]M. Mitomo, ''Pressure Sintering of Si_3N_4,'' *J. Mater. Sci.*, **11**, 1103–107 (1976).

[10]T. Yamada, M. Shimada, and M. Koizumi, ''Densification of Si_3N_4 by High-Pressure Hot-Pressing,'' *Am. Ceram. Soc. Bull.*, **60**, 1281–88 (1981).

[11]T. Yamada, M. Shimada, and M. Koizumi, ''Fabrication of Si_3N_4 by Hot Pressing,'' *Am. Ceram. Soc. Bull.*, **60**, 1225–28 (1981).

[12]I. Tanaka, G. Pezzotti, T. Okamoto, Y. Miyamoto, and M. Koizumi, ''Hot Isostatic Press Sintering and Properties of Silicon Nitride Without Additives,'' *J. Am. Ceram. Soc.*, **72**, 1656–60 (1989).

[13]C. C. Ahn and G. Thomas, ''Microstructure and Grain-Boundary Composition of Hot-Pressed Silicon Nitride with Yttria and Alumina,'' *J. Am. Ceram. Soc.*, **66**, 14–17 (1983).

[14]D. M. Mieskowski and W. A. Sanders, ''Oxidation of Silicon Nitride Sintered with Rare-Earth Oxide Additions,'' *J. Am. Ceram. Soc.*, **68**, C160–C163 (1985).

[15]M. K. Cinibulk and G. Thomas, ''Fabrication and Secondary-Phase Crystallization of Rare-Earth Disilicate–Silicon Nitride Ceramics,'' *J. Am. Ceram. Soc.*, **75**, 2037–43 (1992).

[16]M. K. Cinibulk, G. Thomas, and S. M. Johnson, ''Strength and Creep Behavior of Rare-Earth Disilicate–Silicon Nitride Ceramics,'' *J. Am. Ceram. Soc.*, **75**, 2050–55 (1992).

[17]M. K. Cinibulk, H.-J. Kleebe, G. A. Schneider, and M. Rühle, ''Amorphous Intergranular Films in Silicon Nitride Ceramics Quenched from High Temperatures,'' *J. Am. Ceram. Soc.*, **76**, 2801–808 (1993).

[18]M. N. Menon, H. T. Fang, D. C. Wu, M. G. Jenkins, M. K. Ferber, K. L. More, C. R. Hubbard, and T. A. Nolan, ''Creep and Stress Rupture Behavior of an Advanced Silicon Nitride: Part I, Experimental Observations,'' *J. Am. Ceram. Soc.*, **77**, 1217–27 (1994).

[19]J.-L. Ding, K. C. Liu, K. L. More, and C. R. Brinkman, ''Creep and Creep Rupture of an Advanced Silicon Nitride Ceramic,'' *J. Am. Ceram. Soc.*, **77**, 867–74 (1994).

[20]I. Tanaka, S. Nasu, H. Adachi, Y. Miyamoto, and K. Nihara, ''Electronic Structure Behind the Mechanical Properties of β-Sialons,'' *Acta Metall. Mater.*, **40**, 1995–2001 (1992).

[21]M. K. Cinibulk, G. Thomas, and S. M. Johnson, ''Grain-Boundary-Phase Crystallization and Strength of Silicon Nitride with a YSiAlON Glass,'' *J. Am. Ceram. Soc.*, **73**, 1606–12 (1990).

[22]M. J. Hoffmann, ''High-Temperature Properties of Si_3N_4 Ceramics,'' *MRS Bull.*, 28–32 (1995).

[23]K. K. Richardson, D. W. Freitag, and D. L. Hunn, ''Barium Aluminosilicate Reinforced *In Situ* with Silicon Nitride,'' *J. Am. Ceram. Soc.*, **78**, 2662–68 (1995).

[24]F. F. Lange, ''Relation Between Strength, Fracture Energy and Microstructure of Hot-Pressed Si_3N_4,'' *J. Am. Ceram. Soc.*, **56**, 518–22 (1973).

[25]F. F. Lange, ''Fracture Toughness of Si_3N_4 as a Function of the Initial α-Phase Content,'' *J. Am. Ceram. Soc.*, **62**, 428–30 (1979).

[26]S. H. Knickerbocker, A. Zangvil, and S. D. Brown, ''High-Temperature Mechanical Properties and Microstructures for Hot-Pressed Silicon Nitrides with Amorphous and Crystalline Intergranular Phases,'' *J. Am. Ceram. Soc.*, **68**, C-99–C-101 (1985).

[27]P. F. Becher, S.-L. Hwang, and C.-H. Hsueh, ''Using Microstructure to Attach the Brittle Nature of Silicon Nitride Ceramics,'' *MRS Bull.*, 23–27 (1995).

[28]P. Sajgalik, J. Dusza, and M. J. Hoffmann, ''Relationship between Microstructure, Toughening Mechanisms, and Fracture Toughness of Reinforced Silicon Nitride Ceramics,'' *J. Am. Ceram. Soc.*, **78**, 2619–24 (1995).

[29]A. J. Pyzik and D. R. Beaman, ''Microstructure and Properties of Self-Reinforced Silicon Nitride,'' *J. Am. Ceram. Soc.*, **76**, 2737–44 (1993).

[30]S. R. Choi and J. A. Salem, ''Crack-Growth Resistance of *In Situ*-Toughened Silicon Nitride,'' *J. Am. Ceram. Soc.*, **77**, 1042–46 (1994).

[31]F. Lee and K. J. Bowman, ''Texture and Anisotropy in Silicon Nitride,'' *J. Am. Ceram. Soc.*, **75**, 1748–55 (1992).

[32]G. Himsolt, H. Knoch, H. Huebner, and F. W. Kleinlein, ''Mechanical Properties of Hot-Pressed Silicon Nitride with Different Grain Structures,'' *J. Am. Ceram. Soc.*, **62**, 29–32 (1979).

[33]R. Raj, ''Fundamental Research in Structural Ceramics for Service Near 2000°C,'' *J. Am. Ceram. Soc.*, **76**, 2147–73 (1993).

[34]L. R. McCreight, H. W. Rauch, and W. H. Sutton, *Ceramic and Graphite Fibers and Whiskers*; p. 93. Academic Press, New York, 1965.

[35]P. F. Becher, E. Y. Sun, C.-H. Hsueh, K. B. Alexander, S.-L. Hwang, S. B. Waters, and C. G. Westmoreland, ''Debonding of Interfaces Between Beta-Silicon Nitride Whiskers and Si–Al–Y Oxynitride Glasses,'' *Acta Mater.*, **44**, 3881–93 (1996).

[36]D. S. Zhou and T. E. Mitchell, ''Dislocations in As-Grown CVD α-Silicon Nitride,'' *J. Am. Ceram. Soc.*, **78**, 3133–36 (1995).

[37]I. E. Reimanis, H. Suematsu, J. J. Petrovic, and T. E. Mitchell, ''Mechanical Properties of Single-Crystal α-Si3N4,'' *J. Am. Ceram. Soc.*, **79**, 2065–73 (1996).

[38]W. C. Oliver and G. M. Pharr, ''An Improved Technique for Determining Hardness and Elastic Modulus Using Load and Displacement Sensing Indentation Experiments,'' *J. Mater. Res.*, **7**, 1564–83 (1992).

[39]K. H. Jack, ''Review—Sialons and Related Nitrogen Ceramics,'' *J. Mater. Sci.*, **11**, 1135–58 (1976).

[40]J. W. Harding and I. N. Sneddon, ''The Elastic Stresses Produced by the Indentation of the Plane Surface of a Semi-Infinite Elastic Solid by a Rigid Punch,'' *Proc. Cambridge Philos. Soc.*, **41**, 16–26 (1945).

[41]I. N. Sneddon, ''The Relation Between Load and Penetration in the Axisymmetric Boussinesq Problem for a Punch of Arbitrary Profile,'' *Int. J. Eng. Sci.*, **3**, 47–57 (1965).

[42]R. B. King, ''Elastic Analysis of Some Punch Problems for a Layered Medium,'' *Int. J. Solids Struct.*, **23**, 1657–64 (1987).

[43]R. C. Weast (Ed.), *CRC Handbook of Chemistry and Physics*; p. F-80. CRC Press, West Palm Beach, FL, 1978.

[44]R. W. Hertzberg, *Deformation and Fracture Mechanics of Engineering Materials*; p. 7. Wiley, New York, 1989.

[45]J. F. Nye, *Physical Properties of Crystals*; p. 145. Oxford Science Publications, New York, 1985.

[46]H. Gao, C.-H. Chiu, and J. Lee, ''Elastic Contact versus Indentation Modeling of Multilayered Materials,'' *Int. J. Solids Struct.*, **29**, 2471–92 (1992).

[47]E. Y. Sun, P. F. Becher, S.-L. Hwang, S. B. Waters, G. M. Pharr, and T. Y. Tsui, ''Properties of Silicon–Aluminum–Yttrium Oxynitride Glasses,'' *J. Non-Cryst. Solids*, **208**, 162–69 (1996).

[48]J. J. Vlassak and W. D. Nix, ''Indentation Modulus of Elastically Anisotropic Half Spaces,'' *Philos. Mag. A*, **67**, 1045–56 (1993).

[49]J. J. Vlassak and W. D. Nix, ''Measuring the Elastic Properties of Anisotropic Materials by Means of Indentation Experiments,'' *J. Mech. Phys. Solids*, **42**, 1223–45 (1994).

[50]A. P. Boresi and K. P. Chong, *Elasticity in Engineering Mechanics*; pp. 251–55. Elsevier, New York, 1987.

[51]G. Simmons and H. Wang, *Single Crystal Elastic Constants and Calculated Aggregate Properties: A Handbook*. M.I.T. Press, Cambridge, MA, 1971.

[52]A. Reuss, ''Berechnung der Fliessgrenze von Mischkristallen auf Grund der Plastizitätsbedingung für Einkristalle,'' *Z. Angew. Math. Mech.*, **9**, 49–58 (1929).

[53]W. Voigt, *Lehrbuch der Krystallphysik*; p. 962. B. G. Teubner, Leipzig, Germany, 1928. □